Influence of nanoparticle processing and additives on PES casting solution viscosity and cast membrane characteristics

Lauren F. Greenlee [a, b, *], Nikki S. Rentz [a]

[a] Applied Chemicals and Materials Division, National Institute of Standards & Technology, 325 Broadway, MS 647, Boulder, CO 80305, USA
[b] Ralph E. Martin Department of Chemical Engineering, 3202 Bell Engineering Center, University of Arkansas, Fayetteville, AR 72701, USA

ARTICLE INFO

ABSTRACT

Nanoparticle stabilizer type, casting solution additives, and nanoparticle processing by centrifugal or magnetic separation were varied, and specific membrane characteristics were evaluated. Specifically, membrane casting solution viscosity, cast membrane thickness, pure water flux, and internal morphology were evaluated. While the addition of the additives ethanol and polyvinylpyrrolidone to a polyethersulfone-dimethylacetamide solution causes an expected increase in viscosity, the addition of nanoparticles can cause an increase or decrease in viscosity depending on the ligand stabilizer used during nanoparticle synthesis and casting solution additive concentration. Viscosity can also be affected by nanoparticle separation method, but again, changes are also dependent on casting solution composition. Varying changes in membrane thickness are observed and can be correlated to viscosity. Pure water flux decreases for all samples when nanoparticles are added, but the extent of the change is affected by casting solution composition. Internal morphology can partially explain the decrease in flux for nanoparticle-embedded membranes.

1. Introduction

Nanoparticle incorporation into porous polymeric membranes has received continued attention [1,2,4—17] with the concurrent continued development of reactive metallic and metal oxide nanoparticles for water treatment applications [18—26]. Nanoparticles comprised of metals such as iron, nickel, palladium, silver, aluminum, and copper have been shown to remove both organic [27—30] and inorganic [31—33] water contaminants, and novel multi-metallic nanoparticle combinations (e.g. [34]), and morphologies (e.g. [35]), continue to be reported. Iron nanoparticles (Fe NPs) remain at the forefront of efforts focused on water remediation due to the low cost of the metal and the versatility of Fe NPs in addressing a wide variety of water contaminants [36,37]. The incorporation of these nanoparticle materials into a support material such as a polymeric membrane immobilizes the nanoparticles, preventing movement within the treatment system, and may also provide enhanced contaminant removal. In particular, there is an interest in embedding nanoparticles in phase inversion polymeric membranes, where the nanoparticles can be incorporated into the membrane casting solution and retained in the solid membrane phase when the membrane polymer precipitates.

The majority of work thus far on nanoparticle incorporation into polymeric membranes has focused on the effect of nanoparticle concentration on the polymer casting solution viscosity and subsequent membrane properties such as membrane thickness, morphology, and pure water flux [1,9,10,38—43]. Generally, an increase in nanoparticle concentration will cause an increase in casting solution viscosity [41,43]. Depending on the balance between kinetic and thermodynamic effects during phase inversion, nanoparticle addition can cause either an increase or decrease in membrane porosity or pore size, with correlated changes in membrane performance. However, other properties or aspects of nanoparticle synthesis and processing may also affect the membrane casting solution and resulting polymer membrane. Most iron-based nanoparticles are synthesized by reduction of an iron salt precursor in aqueous solution, and different types of organic ligands and polymers are used to stabilize the nanoparticle suspension [19,24,44—46]. These nanoparticle stabilizers are subsequently adsorbed to the nanoparticle surface and will be present when the nanoparticles are incorporated into a membrane matrix. Additionally, synthesized nanoparticles must be separated from the

* Corresponding author.
E-mail address: greenlee@uark.edu (L.F. Greenlee).

synthesis solution, and often go through several processing steps (e.g., centrifugation, solvent rinses, drying, annealing). These aspects of nanoparticle synthesis and processing are known to change nanoparticle reactivity [47–50] and may change the properties and performance of a subsequent nanoparticle-embedded membrane; however, few studies have attempted to investigate how nanoparticle stabilizers and particle processing methods affect nanoparticle-polymer solutions and cast membranes.

Phase inversion membranes are often cast from polymer-solvent solutions that also have additional additives, including pore-former compounds such as polyvinylpyrrolidone (PVP) and non-solvent compounds such as ethanol [51–56]. While the impacts of such additives on the phase inversion process and resulting membrane formation are well-known, the influence of nanoparticles in an additive-polymer-solvent system is also unexplored.

In this study, polyethersulfone (PES) membranes were cast from the solvent dimethylacetamide (DMAC) by phase inversion in a water bath. The PES polymer concentration in DMAC was held constant at 15 wt %, and the addition of stabilized iron nanoparticles, PVP, and ethanol to the membrane casting solution and cast membranes was evaluated. Two different nanoparticle stabilizers, the polymer carboxymethyl cellulose (CMC) and the chelator aminotris(methylene phosphonate) (ATMP), were used, and synthesized nanoparticles were of similar size for both stabilizers, albeit with different calculated average diameters and diameter ranges. Nanoparticles were separated from the synthesis solution by either centrifugation or magnetic separation. Viscosity measurements were used to characterize casting solutions, while membrane thickness and pure water flux were used to evaluate changes to cast membranes as a function of additive type and concentration. The effects of the addition of PVP and/or ethanol on solution viscosity and resulting membrane thickness and flux are expected; both additives cause an increase in viscosity and a decrease in pure water flux. However, the addition of nanoparticles to casting solutions containing PVP and/or ethanol resulted in varying trends. The type of nanoparticle stabilizer used and the method of nanoparticle separation both affected casting solution and membrane properties. Electron microscopy results for internal membrane morphology are reported in Supplemental Material.

2. Materials and methods

2.1. Chemicals

All chemicals were used as received and were commercially purchased as ACS grade, unless otherwise noted. Aminotris(methylene phosphonate) (ATMP, obtained from Dequest Water Solutions, molecular weight = 298 g/mol) and carboxymethyl cellulose (CMC, molecular weight = 250,000 g/mol) were used as nanoparticle ligand stabilizers. Iron sulfate heptahydrate (Fe$_2$SO$_4$*7H$_2$O) was used as the salt precursor for iron nanoparticle synthesis. Sodium borohydride (NaBH$_4$) was used in powder form. Concentrated nitric acid (HNO$_3$) was used to make 10% HNO$_3$ for cleaning glassware. Polyethersulfone (PES) (Veradel 3100P) was obtained from Solvay Polymers. Polyvinylpyrrolidone (PVP, molecular weight = 40,000 g/mol) and ethanol (100%, no additives) were used as casting solution additives. Dimethylacetamide (DMAC) was used as the casting solution solvent for all membrane casting solutions.

2.2. Nanoparticle synthesis & characterization

Ligand-stabilized iron nanoparticles were synthesized as previously reported [57,58]. Briefly, a borosilicate three-neck flask was soaked in 10% nitric acid overnight and subsequently rinsed four times with deionized water. The nanoparticle synthesis solution was then added to the three-neck flask; the starting solution included iron precursor FeSO$_4$*7H$_2$O at a concentration of 10 g/L as Fe in deionized water and a ligand stabilizer. ATMP was used at a molar ratio of 0.05 ATMP:Fe and CMC was used at a molar ratio of 0.0001 CMC:Fe. While these ratios are quite different, when the ratio is calculated on the basis of functional groups (carboxyl in CMC and phosphate in ATMP), the molar ratio of associating functional group to iron is quite similar. While ATMP has three phosphate groups, the ATMP molecule is known to associate with only one iron atom in solution [59]. In previous work, these ratios for ATMP and CMC produced similarly-sized iron nanoparticles [57,60] and thus are used in this study to have nanoparticles in the same size range that have two different surface-sorbed ligands. The nanoparticle synthesis solution was bubbled for 15 min under argon to remove dissolved oxygen, with mixing provided by an orbital shaker. Then a fresh solution of NaBH$_4$ was added dropwise by a syringe while the flask was hand-mixed for a final molar ratio of 2.2 BH$_4$:Fe. This molar ratio was chosen based on the theoretical requirement of 2 mol BH$_4$ per mol of Fe^{2+} for complete reduction of all Fe^{2+} atoms, with an additional 10% excess added to account for the side reaction of BH$_4^-$ with water that also occurs once NaBH$_4$ is in solution [61].

Once the NaBH$_4$ was added to the synthesis solution, the flask was returned to the orbital shaker and mixed under vacuum for 15 min. The resulting nanoparticles were separated from the remaining dissolved salts and excess stabilizer in the synthesis solution through two methods, either magnetic separation or centrifugation. The two separation methods were not used together, but rather, the same type of nanoparticle sample (either ATMP-stabilized or CMC-stabilized) was separated by magnetic separation, and then a repeat sample of nanoparticles was separated by centrifugation. The same set of membrane casting conditions was then tested for each separation method to determine the effect of the nanoparticle separation method on membrane properties. For magnetic separation, the nanoparticle solution was placed in a 50 mL conical tube, and a magnet was placed underneath the tube. Once the nanoparticles formed a pellet at the bottom of the tube, the supernatant was pipetted off of the pellet and replaced with ethanol. For centrifugal separation, the nanoparticle solution was centrifuged for 1 h at 18,000 rcf, the supernatant was removed, and the remaining nanoparticles were resuspended in ethanol for storage. Nanoparticles were resuspended in ethanol by sonication on ice for 30 min. Nanoparticles were imaged using a field emission scanning electron microscope (FESEM).

2.3. Casting solutions & membrane casting

All membrane casting solutions were comprised of 15 wt % PES in DMAC, and all membranes were cast at a relative humidity of <30%. Casting solutions were typically made in volumes of 2–5 mL and were stored in Teflon-capped scintillation vials prior to casting. Casting solution additives included the pore-former PVP and the non-solvent ethanol; PVP was tested at concentrations of 0–2 wt %, and ethanol was tested at concentrations of 0–25 wt %. Nanoparticle-ethanol suspensions were centrifuged for 30 min at 18,000 rcf, the ethanol supernatant was removed, and DMAC was added at the specific volume required depending on the target nanoparticle concentration in the casting solution. Nanoparticles were tested at a nanoparticle concentration of 1 wt %. The addition of nanoparticle mass to the casting solution was based on the starting synthesis solution concentration of 10 g/L as Fe; some loss of nanoparticles likely occurs during the transfer of nanoparticles from the synthesis flask to the storage solution; however, the loss is expected to be the same for all casting solution compositions

because all nanoparticles were synthesized the same way in replicate batches. Therefore, the trends observed in casting solution and membrane properties can still be evaluated for the set of experiments performed.

Membranes were cast onto a glass plate that was cleaned with deionized water and isopropanol. A two-inch wide doctor blade and an automated caster was used, and all membranes were cast at 150 μm blade height. Once the casting solution was drawn out on the glass plate, the plate was immediately placed into a deionized water bath such that the water completely covered the cast solution. Typically, the PES membrane formed within several seconds, and floated off of the glass plate. The membrane was then sectioned for thickness and flux measurements; a one-inch steel hole punch was used to cut membrane samples for dead-end pure water flux experiments. All membrane sections were stored in ethanol between casting and thickness/flux measurements. Membrane samples were never permitted to dry out between casting and subsequent characterization.

2.4. Rheometry

A commercial viscometer was used for all rheometry measurements, and all measurements were performed with a cone-and-plate fitting and a 1 mm gap in between the cone and plate. All measurements were performed on 800 μl casting solution samples at 20 °C. The viscosity of each solution was measured over a shear rate range of 600 s^{-1} to 1000 s^{-1}, and 10 data points were taken within that shear rate range. At least two separate measurements were made on each casting solution, and the viscosity averages reported herein are based on duplicate viscosity measurements over the entire shear rate range, unless otherwise noted.

2.5. Low-force micrometer measurement

A commercial low-force micrometer was used to measure the cast membrane thickness. At least five separate thickness measurements were taken on each membrane sample, and each measurement was taken at a different random location on the membrane to take into account any spatial variation in thickness as a result of membrane casting heterogeneity. For each sample, a membrane was removed from the ethanol storage solution, excess ethanol was removed with a kimwipe, and the membrane thickness was measured while the membrane remained wet. The membrane was then replaced into the ethanol storage solution.

2.6. Pure water flux measurement

Pure water flux was measured in a dead-end filtration setup at a pressure of 0.7 bar. The filtration setup included a 20 mL dead-end cell that was connected to a 1 L pressurized reservoir. A one-inch membrane sample was placed on top of a one-inch 0.45 μm filter support and held in place in the base of the dead-end cell by a Viton o-ring. Deionized water was used for all measurements. The filtered water was collected in a beaker on a digital mass balance, and an in-house Labview program was used to record accumulated mass as a function of time (every five seconds). Pure water flux was then calculated based on the surface area of the membrane sample.

3. Results and discussion

3.1. Nanoparticle synthesis

Iron nanoparticles were synthesized with each stabilizer (CMC or ATMP), and representative FESEM images are shown in Fig. 1. The two representative stabilizers were chosen due to the common use

of CMC as a water soluble stabilizer for aqueous-based iron nanoparticle synthesis [45,62–65] and our previous results demonstrating the applicability of phosphonate-based chelator compounds as successful stabilizers for iron nanoparticles [57,58]. Prior results have shown that the type of stabilizer used can affect nanoparticle properties such as size and morphology [57], but also properties such as reactivity and oxidation kinetics [60]. It is therefore likely that the stabilizer used will also have an impact on membrane properties, even if all other aspects of nanoparticle composition and morphology are the same. Visually, nanoparticle size and size dispersity appear to be slightly different for the two different stabilizers; the ATMP-stabilized iron nanoparticles appear to be less polydisperse but with a larger overall size, while the CMC-stabilized iron nanoparticles appear to have particles that are both smaller and larger than the ATMP-stabilized iron nanoparticles. These results suggest that as a stabilizer, ATMP enables the synthesis of nanoparticles with better size control than when CMC is used. This difference is likely due to the significantly different structures of ATMP versus CMC, where all ATMP molecules have the same molecular structure and act as chelators to iron. In contrast, CMC is a long-chain polymer with a known molecular weight but with variable substitution of carboxymethyl groups for hydroxyl groups on the cellulose polymer backbone. The multiple, different substitution sites on the cellulose backbone would result in individual polymer chains with varying degrees of coordination to iron, with subsequent variation in controlling nanoparticle precipitation and growth. To evaluate nanoparticle size further, the FESEM images were analyzed with ImageJ software to quantify the average and standard deviation of nanoparticle size for each stabilized sample. For each image, 40 separate particle diameter measurements were made. The average nanoparticle size for ATMP-stabilized iron nanoparticles was 128 nm ± 25 nm, and the average nanoparticle size for CMC-stabilized iron nanoparticles was 94 nm ± 46 nm. These results are similar to those previously reported [58]. While the calculated average nanoparticle diameter is different, the size ranges of each nanoparticle sample overlap, and compared to the range of nanoparticle sizes reported in literature [44,58,66–68], which can range from several nanometers to hundreds of nanometers, the two nanoparticle samples reported here are considered to be similar in size.

Nanoparticle morphology was similar for both stabilizers, and based on previous results from the same synthesis procedure, the nanoparticles are assumed to be comprised primarily of iron metal with a passivating oxide shell [58,60,69,70]. Due to the large size of the nanoparticles, the passivating oxide is expected to protect the inner iron core and prevent continued iron oxidation after a thickness of several nanometers is reached [71]. The passivating oxide generally remains stable unless exposed to an agitated environment of oxygen and water; for example, when iron nanoparticles are exposed to flowing oxygenated water, the particles will oxidize to an iron oxyhydroxide within a period of 10 min [60]. If oxidation occurs, a distinct visual color change occurs, with the sample going from a dark black color to a bright orange color. While direct measurement of nanoparticle metal phase was not performed for this study, no visual color changes were observed during nanoparticle processing, casting solution preparation, or membrane casting. Cast membranes containing nanoparticles always had a distinct dark gray color. In addition, the nanoparticle morphology changes significantly from spherical particles to elongated crystallites [60]; this crystallite morphology is not observed in the images shown in Fig. 1, nor in nanoparticles imaged within the internal membrane morphology (Supplemental Material, Fig. S2). As a result, we assume that the nanoparticles incorporated into the casting solutions and in cast membranes remained intact as iron metal core-oxide shell particles, but additional
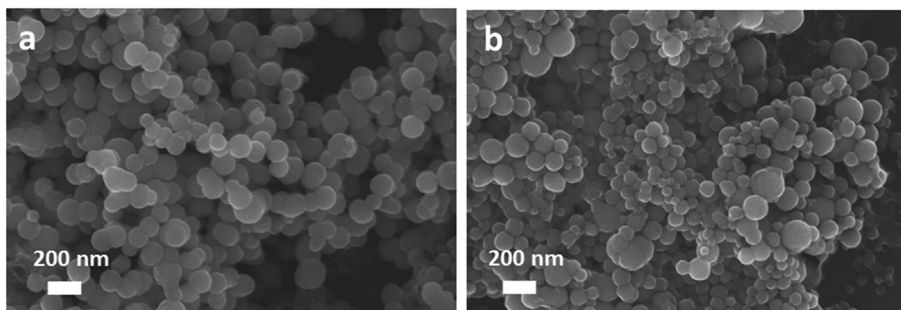
Fig. 1. FESEM images of (a) ATMP-stabilized Fe NPs and (b) CMC-stabilized Fe NPs.

measurements would be needed to confirm these observations.

3.2. PES membranes: addition of PVP and ethanol as additives

Casting solutions that did not contain nanoparticles and that were composed of simple combinations of PES polymer and DMAC solvent tended to result in a relatively flat linear relationship between viscosity and shear rate. When additives such as ethanol and/or PVP were added to the casting solution, slight decreases in viscosity were observed as the shear rate increased. Ethanol was tested for concentrations between 1 wt % and 25 wt %, and PVP was tested at a concentration of 2 wt %. Overall, the decrease in viscosity varied from 0% to 9% over the shear rate range, with the addition of ethanol appearing to have more of an effect than PVP on changes to viscosity as a function of shear rate.

The sample set of membrane casting solutions without nanoparticles produced expected trends (Fig. 2), and the results were similar to those already reported in the literature [51,52,54,72]. When 2 wt % PVP was added to the casting solution (composed of 2 wt % PVP, 15 wt % PES, and 83 wt % DMAC), the viscosity increased from 0.095 Pa s to 0.14 Pa s. The addition of ethanol also caused an increase in casting solution viscosity, and the combination of
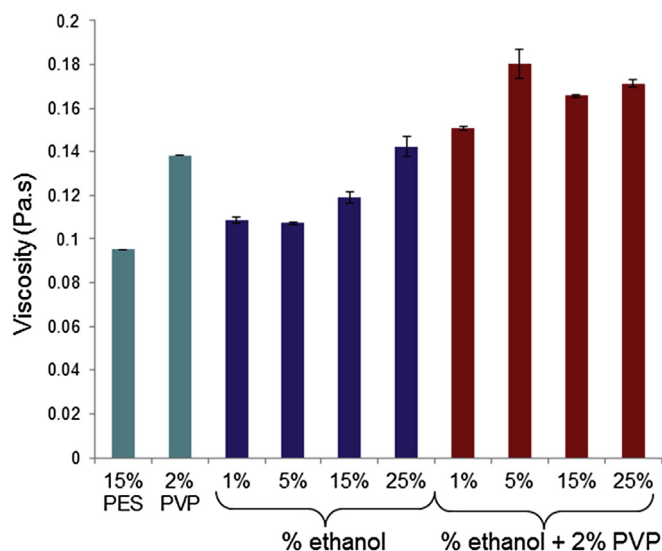
ethanol and PVP caused an even greater increase in solution viscosity than addition of either additive alone. However, when PVP was present in the solution, the rate of increase in viscosity as a function of ethanol concentration was less than for solutions that did not contain PVP. In other words, when a linear regression analysis is performed on viscosity as a function of ethanol concentration, the viscosity increases at a rate of 0.016 Pa s per unit wt % ethanol for solutions containing ethanol, PES and DMAC, whereas the viscosity increases at a rate of 0.012 Pa s per unit wt % ethanol for solutions with PVP, ethanol, PES, and DMAC. Overall, the increase in viscosity with PVP and ethanol is an expected trend and forms the control set of experiments for subsequent experiments with nanoparticle-loaded casting solutions.

While both of the additives cause an increase to the PES/DMAC solution viscosity, the mechanisms by which a non-solvent such as ethanol and a polymer such as PVP cause an increase in viscosity are quite different. When a non-solvent such as ethanol is added, the solvent DMAC is soluble in the non-solvent ethanol, but PES is not soluble in ethanol. As a result, the addition of ethanol reduces the interaction between PES and DMAC, and PES effectively has less solvent in which to be dissolved. A higher effective polymer concentration causes the polymer chains to be less extended and in a more compact, coiled conformation [51,73,74]. This change in polymer conformation and reduction in available solvent also increases polymer–polymer interactions such as chain entanglement, thus increasing the viscosity of the overall solution. When a polymer additive such as PVP is added, the two polymers, PES and PVP in this case, interact and become entangled [52]. For the specific case of PES and PVP, the Flory–Huggins interaction parameter has been determined to be less than zero, suggesting that the polymers are highly miscible and form homogeneous blends at all concentrations [52]. At thermodynamic equilibrium, the two polymers would separate, and the additive PVP would move to the interface between the precipitated PES polymer and the polymer-lean solvent phase [52]. However, the time scale for this process is much slower than the time scale for non-solvent bath diffusion into and solvent diffusion out of the cast polymer solution [52]; as a result, the polymers stay entangled, and the added polymer mass and entanglement causes an increase in the polymer solution viscosity.

3.3. Nanoparticle addition to PES membranes: PVP and ethanol additives

Casting solutions containing nanoparticles were then compared to the set of control solutions that contained only PES and additives ethanol and/or PVP. All solutions with nanoparticles were tested at a nanoparticle concentration of 1 wt %. Both sets of nanoparticles were tested: iron nanoparticles stabilized with CMC and iron nanoparticles stabilized with the metal chelator ATMP. The purpose

Fig. 2. Effect of membrane casting solution additives PVP and ethanol on casting solution viscosity for solutions without nanoparticles. All solutions contained 15 wt % PES in DMAC and were tested at 20 °C. The molecular weight of the PVP used was 40,000 g/mol. Moving from left to right across the figure, labels beneath the bar graph represent additions to the casting solution composition. The first bar on the left is for a casting solution of 15 wt % PES in DMAC, and the second bar from the left is for a casting solution of 15 wt % PES, 2% PVP in DMAC.

of this study was to investigate whether the stabilizer that is adsorbed to the surface of the nanoparticles will have a significant influence on casting solution and membrane properties, as well as to determine the role of additives. Polymers and small molecule chelators are two key types of ligands used as nanoparticle stabilizers during aqueous synthesis, and CMC and ATMP were chosen to represent these two stabilizer categories for this study. While the molar ratios of stabilizer to iron are quite different for CMC versus ATMP, the two molar ratios used equate to approximately the same number of functional coordinating groups per mole of iron (carboxyl groups in CMC and phosphate groups in ATMP). While both CMC and ATMP are hydrophilic and contain charged functional groups, the CMC polymer will likely form a larger steric organic layer on the surface of the nanoparticles, whereas the small ATMP molecule is likely to form a thinner, low-mass organic layer on the nanoparticle surfaces [58,70]. The differences in these two surface coatings and how the two stabilizer molecules interact with the polymer casting solution will necessarily affect how the addition of nanoparticles changes the casting solution and cast membrane. While a more extensive study is certainly needed to delineate the details of how different stabilizer properties affect nanoparticle-embedded membrane formation, the initial results presented herein demonstrate that the type of stabilizer on the nanoparticle surface does affect casting solution viscosity and membrane properties, for the same nanoparticle material.

Viscosity measurements of nanoparticle-loaded casting solutions are shown in Fig. 3, where the stabilizer choice appears to have a significant effect on the casting solution viscosity. However, trends as a function of stabilizer type and with the addition of PVP and ethanol vary. If the viscosity of a solution of 15% PES in DMAC (Fig. 2, left-most bar, 0.095 Pa s) is compared with the viscosity of the same solution with either CMC-stabilized iron nanoparticles or ATMP-stabilized iron nanoparticles added (Fig. 3, left-most set of two bars), the CMC-stabilized nanoparticles cause the viscosity to decrease to 0.060 Pa s, whereas the ATMP-stabilized nanoparticles cause the viscosity to increase to 0.11 Pa s. When ethanol and PVP are added to the nanoparticle-loaded casting solutions, the viscosity generally increases, but a systematic increase in viscosity with an increase in ethanol or PVP concentration, as is observed for nanoparticle-free solutions, is not obtained. For solutions with

ethanol added as an additive, the presence of ATMP-stabilized nanoparticles caused larger increases in viscosity as compared to CMC-stabilized nanoparticles, except for the highest ethanol concentration of 25 wt %. Within the ethanol concentration range tested (1 wt % to 25 wt %), in general, the viscosity decreased with increasing ethanol concentration for ATMP-stabilized nanoparticles, while the opposite trend is observed for CMC-stabilized nanoparticles. When 2 wt % PVP is added to the four ethanol concentrations, the two nanoparticle types displayed a similar trend; the viscosity decreases from 1 wt % to 15 wt % ethanol, but then increases for 25 wt % ethanol. None of the trends observed for nanoparticle-added solutions are the same as the typical trends observed with casting solution additive concentration (Fig. 2).

For nanoparticle-added casting solutions, there was typically a decrease in the viscosity as a function of shear rate, and the CMC-stabilized nanoparticles appear to have a greater effect on the decrease in viscosity than the ATMP-stabilized nanoparticles. In addition, greater changes in viscosity as a function of shear rate were observed for higher additive concentrations (e.g., 15–25 wt % ethanol). For lower additive concentrations, viscosity decreased within the range of 3–10%, whereas for higher ethanol concentrations and in the presence of PVP, viscosity decreases ranged from 10 to 30%. For this study, only average viscosities are reported because a greater shear rate range, temperature range, and additive concentration range would need to be studied to further delineate the effect of nanoparticles and additives on shear-induced viscosity changes [75,76]. Furthermore, the experimental setup used herein did not include a solvent trap, which is typically necessary to ensure accurate analysis of non-Newtonian behavior [75,76]. Future work would include a study on viscosity as a function of polymer concentration and nanoparticle concentration to further study shear thinning and non-Newtonian behavior. For this study, viscosities were taken as average values and used to understand the effects of nanoparticle and casting solution additive additions.

The anomalous trends as a function of casting solution additive concentration when nanoparticles are added may be the result of both nanoparticle behavior within the solution and interactions between the nanoparticles and the components of the solution. Generally, the addition of a non-solvent like ethanol or a hydrophilic additive such as PVP increases the viscosity of the casting solution because these additives do not generally dissolve or mix well, respectively, with the membrane polymer (PES in this case). PES is more hydrophobic than PVP; PES is only soluble in solvents such as DMAC or dimethylformamide (DMF), whereas PVP is water-soluble. As a result, these additives effectively reduce the volume of DMAC available in the solution for PES dissolution, and the solution viscosity increases. Nanoparticles may act in the same way, effectively reducing the volume available for PES. However, nanoparticles might also cause changes in polymer conformation depending on nanoparticle size and surface composition (i.e., surface-sorbed ligand properties). Furthermore, the stability of the nanoparticles themselves will be affected by the casting solution composition; there may be more or less particle agglomeration depending on nanoparticle-solvent-additive interactions. All of these factors will affect the resulting solution viscosity, and several contributing factors most likely are influencing the viscosity trends observed in Fig. 3.

There are several potential mechanisms for why the addition of nanoparticles can cause a change in viscosity. Two trends can be evaluated: the effect of increasing additive concentration with and without nanoparticles, and the addition of one of the two different nanoparticle types for a particular composition and how the stabilizer might possibly be affecting viscosity. Generally, when CMC-stabilized nanoparticles are added to the polymer solution, the viscosity decreases in comparison to the nanoparticle-free solution.
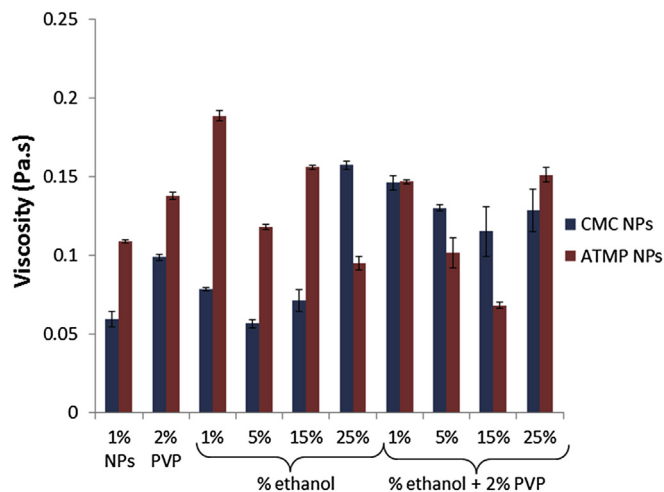

Fig. 3. Effect of the nanoparticle stabilizer type on casting solution viscosity. CMC and ATMP nanoparticle stabilizers were tested at ratios of 0.0001 mol CMC:mol Fe and 0.05 mol ATMP:mol Fe. The molar ratios of CMC:Fe and ATMP:Fe are equivalent to approximately 0.15 mol chelating groups per mol Fe. The molecular weight of CMC was 250,000 g/mol. All measurements were taken at 20 °C.

Within the set of samples that all contained CMC-stabilized nano-particles, the trend with the additions of ethanol or PVP does not follow that of the nanoparticle-free data set. It appears that except for the case of 25% ethanol, the presence of CMC decreases the viscosity. If this effect is considered within the context of the molecular picture of how ethanol and PVP cause an increase in the viscosity (i.e., a reduction in available solvent for solvent–polymer interactions and increased polymer–polymer entanglement interactions, respectively) it is possible that the presence of the nanoparticles, and in particular with CMC as a stabilizer, counteracts these mechanisms. CMC is soluble in a non-solvent such as ethanol, and the large physical volume of the CMC polymer around the surface of the nanoparticles could absorb a significant volume of the ethanol added, such that the ethanol is not available for interaction with DMAC and more of the DMAC remains available for solvent-PES polymer interaction. This effect would essentially increase the PES/DMAC volume and allow PES to be in solution in DMAC at a lower effective concentration, causing a decrease in solution viscosity. This mechanism is overcome at the higher ethanol concentration of 25 wt %, where an increase in viscosity is observed with the addition of nanoparticles, as compared to the nanoparticle-free solution. The effect on PVP addition could be similar, where CMC-PVP interactions decrease PVP-PES interactions. Since CMC and PVP are both hydrophilic polymers, it is likely that their interactions would be stronger than those of PVP and PES. The trend for CMC-stabilized nanoparticles within the ethanol or PVP data sets suggests that up to a certain concentration of additive, the addition of more additive causes an additional decrease in viscosity. This may be an interaction saturation effect, where the CMC polymer can continue to interact with additional ethanol molecules or PVP molecules up to a certain concentration, but eventually a saturation limit is reached, and subsequent addition of additive causes an increase, instead of a decrease, in viscosity.

If ATMP-stabilized nanoparticles are then considered, the addition of ATMP-stabilized nanoparticles to the ethanol-containing polymer solutions generally caused an increase in viscosity above that of the nanoparticle-free solutions. This behavior is consistent with previously reported results showing an increase in viscosity with the addition of nanoparticles [77]. Nanoparticles can act in a similar manor to a non-solvent such as ethanol when the surface of the nanoparticles is hydrophilic (as it is for iron nanoparticles with CMC or ATMP stabilization [69,70]), where the nanoparticles cause nanoparticle–solvent interactions. This effect decreases PES-solvent interactions and causes a further decrease in the available volume of solvent for polymer dissolution and a further increase in the apparent viscosity of the overall solution. When ATMP-stabilized nanoparticles are added to PVP-containing PES solutions, there is little to no increase in viscosity, and in fact, decreases in viscosity are observed. Due to the hydrophilic nature of the ATMP, it appears that the addition of nanoparticles causes interactions between the nanoparticles and the PVP, such that the typical effect of adding nanoparticles and an increase in viscosity is not observed. Similar to the effect observed for CMC-stabilized nanoparticles, the nanoparticle-PVP interactions likely decrease the PES-PVP interactions, decreasing the effect of the additive on the overall solution viscosity. Overall, the results obtained for nanoparticle-incorporated polymer solutions demonstrate that the addition of nanoparticles can be used to increase or decrease the solution viscosity depending on the other solution components and concentrations. The addition of hydrophilic nanoparticles to a more hydrophobic polymer system also can be highly dependent on the nature of the surface-sorbed nanoparticle stabilizer.

The effect of nanoparticle addition on cast membrane thickness is shown in Fig. 4 for both nanoparticle-free and nanoparticle-
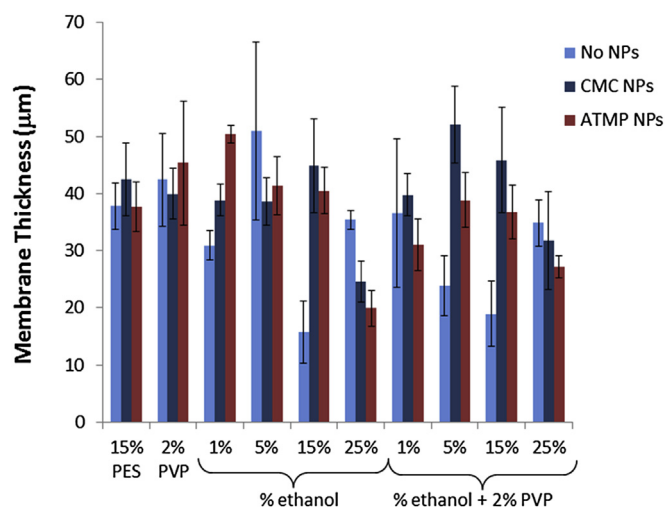

Fig. 4. Effect of nanoparticles and nanoparticle stabilizer type on cast membrane thickness.

embedded membranes. Cross sectional images for all cast membranes are reported in Supplemental Information. A single-factor ANOVA analysis of the membrane thickness data for the three cases of no nanoparticles, CMC-stabilized nanoparticles, and ATMP-stabilized nanoparticles resulted in no statistical difference between these three data sets. Therefore, the addition of nanoparticles to the casting solution does not significantly change the resulting membrane thickness. This result is important in attempting to understand how the addition of nanoparticles affects membrane water flux (Fig. 5), where the differences in measured flux are clearly due to mechanisms other than a change in membrane thickness. Within one data set of membrane thickness (e.g., all membranes cast with no nanoparticles or CMC-stabilized nanoparticles) the changes in thickness with the addition of ethanol and PVP are statistically significant for each data set. Similar results were observed by Amirilargani and Mohammadi for the addition of the non-solvents ethanol and 1-propanol to PES polymer solutions in N-methyl-2-pyrrolidone (NMP) [51]. While
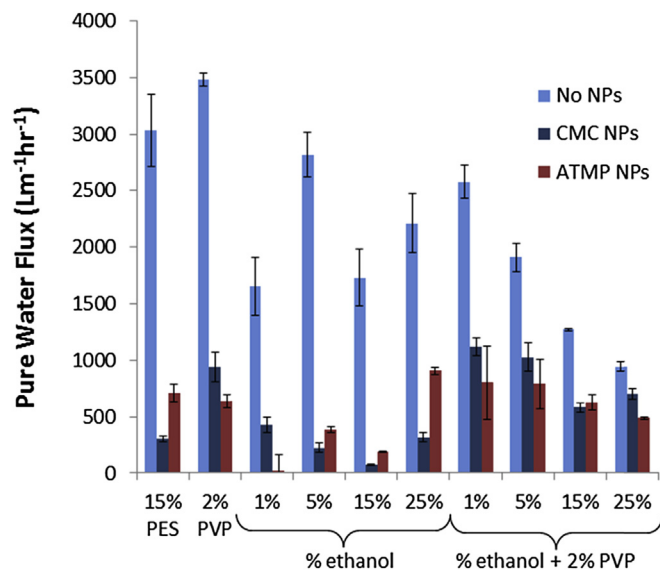

Fig. 5. Effect of nanoparticles and nanoparticle stabilizer type on membrane pure water flux.

the authors did not quantitatively evaluate membrane thickness as is presented in Fig. 4, the cross-sectional images reported show a similar trend: with smaller additions of non-solvent (5–10 wt %), the membrane thickness increases, while at higher mass additions (15–20 wt %), the membrane thickness then appears to decrease [51]. Torrestiana-Sanchez et al. also observed a measured increase in membrane thickness with non-solvent (H_2O) additions of 5–7.5 wt % [78].

Changes in cast membrane thickness are related to changes in casting solution viscosity, where both thermodynamic and kinetic arguments are known to play a role in membrane formation [52,54]. Often these different aspects counteract each other, so the change in membrane thickness depends on which effect is dominant during phase inversion. Furthermore, the specific combination of non-solvent or polymeric additive, polymer, and solvent will influence how the membrane thickness and viscosity change for a given system [51,52,78,79]. In the system presented herein, when the casting solution viscosity increases at lower non-solvent mass additions (1–5% ethanol addition), the solution is essentially thicker, and the inward diffusion of water and the outward diffusion of solvent are slowed. However, the increase in viscosity due to additive addition also causes the solution to be closer to thermodynamic instability (i.e., PES precipitation), which would cause faster polymer precipitation during phase inversion. Typically, if phase inversion is slowed, the polymer chains have more time to rearrange and the formed membrane tends to be thicker, whereas faster phase inversion results in thinner membranes. The time scale for slower phase inversion is on the order of seconds or tens of seconds longer, so the polymer chains do not have enough time to completely extend and disentangle, such as in the polymer die swell phenomenon [80,81]. However, an increase in viscosity caused by the addition of non-solvent may enable phase inversion through polymer precipitate nucleation and growth, rather than by instantaneous spinal decomposition [82], where a metastable polymer-lean phase forms, causing macrovoid formation (observed in the cross-sectional images in Supplemental Information) and growth and giving the polymer in solution a slight increase in time before precipitation. As a result, the coiled polymer chains do not immediately precipitate as coiled, spherical particles but as slightly elongated, entangled chains [83]. This effect can result in a thicker membrane, as is observed for some of the non-solvent concentrations in Fig. 4. As the concentration of additive increases, it is unsurprising that the membrane thickness then decreases as the polymer casting solution is pushed closer towards thermodynamic instability [52,54,82].

Ultimately, the goal with membrane materials development is to connect properties to performance. The primary focus of this study was to develop an understanding of how nanoparticle incorporation affects key properties such as casting solution viscosity and membrane thickness, and to also test the pure water flux of the cast membranes as an initial performance metric. Future work on these membranes will include further performance testing (e.g., rejection of model water contaminants) on a subset of the membranes chosen based on pure water flux performance. Pure water flux performance is an indirect indication of the porosity and relative pore size within the set of membranes tested here (where higher flux suggests a more open pore structure), but large differences in membrane thickness can also impact flux results (i.e., a significant increase in membrane thickness will cause a decrease in flux). Pure water flux results are shown in Fig. 5 for nanoparticle-free and nanoparticle-embedded membranes. In all cases, the addition of nanoparticles causes a decrease in flux, and for many of the casting solution compositions tested, the decrease in flux is dramatic. For the sample set with PVP and ethanol addition, the decrease in flux is less dramatic with nanoparticle addition, and

this sample subset would likely be chosen for future studies to determine how contaminant rejection changes as a result of nanoparticle addition. In an ideal case, nanoparticle addition would enable similar or increased flux with improved contaminant rejection; a slight decrease in flux may be acceptable depending on the contaminant removal performance of the membrane. These pure water flux results suggest that with optimization of casting solution composition (i.e., type and concentration of additive), nanoparticle-embedded membranes may be able to retain flux performance while enabling enhanced removal of water contaminants. As with the viscosity and membrane thickness results, differences are observed as a function of the stabilizer used for nanoparticle synthesis, making stabilizer type also a parameter that can be optimized and tuned for improved membrane performance. The effect of the stabilizer on contaminant removal would also need to be investigated within the context of these nanoparticle-embedded membranes.

The decrease in pure water flux caused by the addition of nanoparticles has been observed in other studies [43,84,85]. Akar et al. observed that the addition of nanoparticles caused a denser pore structure at the surface of the membranes, where the pore size decreased as a result of smaller, more densely packed precipitated polymer structure [43]. The authors explain this result through the mechanism of delayed demixing [43], where the occurrence of a polymer-lean phase allows a slightly longer precipitation time frame and elongation of the polymer chains from a spherical precipitate structure to an entangled matrix, as explained by the work of Boom, Strathmann and co-authors [52,86]. In Fig. S1 (Supplemental Information), a similar increase in the dense packing of the membrane surface structure with the addition of nanoparticles is observed in SEM images of membrane top surfaces. A similar effect on membrane surface structure (Fig. S1) is observed for the addition of ethanol, suggesting the addition of hydrophilic nanoparticles may be similar to the addition of a hydrophilic non-solvent. Both the addition of nanoparticles and the addition of ethanol or ethanol/PVP caused a decrease in pure water flux (Fig. 5).

However, in the results presented in Fig. 5, the addition of nanoparticles causes a much greater decrease in pure water flux than the addition of ethanol, as compared to the nanoparticle-free membranes. Thus, there are likely additional mechanisms involved in how the addition of iron nanoparticles impact the pure water flux of a PES membrane. In the field of gas separations, the effect of nanoparticle fillers on dense polymer membrane permeability of gases has been successfully modeled using the Maxwell and Bruggeman relationships, which were originally developed to explain electrical conductivity and the dielectric constant of composites [87–89]. In general, the addition of a non-porous nanoparticle filler into a polymer membrane can cause an increase in gas permeability without a decrease in gas selectivity, decoupling the traditional permeability-selectivity trade-off [89]. A similar relationship, where the change in permeability is described by the volume fraction of nanoparticles in the polymer matrix, has not been broadly applied or developed for water permeability in nanoparticle-embedded porous microfiltration/ultrafiltration membranes [87]. The general mechanism for the influence of nanoparticles on porous membrane water permeation may be quite different as the addition of nanoparticles often causes a decrease in water flux, as opposed to the results for gas permeability of nanoparticle-embedded polymer membranes. In addition to causing changes in how the dense top surface layer forms, the addition of nanoparticles to a porous polymer membrane may also reduce the available pathways for water flow through the membrane as well as change the internal macrovoid structure that forms (cross-sectional images in Supplemental Information, Figs. S5 and S8). Similar to the occurrence of delayed demixing at the

membrane surface, macrovoid structure is indicative of delayed demixing throughout the thickness of the membrane, where the polymer-lean phase allows growth of the macrovoid structure and may allow the precipitation of a denser polymer-rich phase along the interface of the forming macrovoids. The presence of PVP in nanoparticle-embedded PES (Fig. 5) appears to counteract the presence of the nanoparticles, a result that aligns with this potential mechanism, since PVP is known to increase interconnectivity and openness of PES pore structure [52].

3.4. Nanoparticle addition to PES membranes: magnetic versus centrifugal separation

In addition to casting solution parameters such as additive type and nanoparticle stabilizer, nanoparticle processing steps may affect the casting solution viscosity and membrane properties. In Fig. 6, results are presented for nanoparticle-added membrane casting solutions, where the nanoparticles were processed in two different ways after nanoparticle synthesis. In both cases, the nanoparticles were synthesized with either ATMP or CMC as the stabilizer. To separate the nanoparticles from the synthesis solution, the particles were either magnetically separated or separated through centrifugation. In both cases, the rest of the synthesis solution was removed from the nanoparticle sample, and the nanoparticles were resuspended in DMAC to make the nanoparticle-loaded membrane casting solutions. Centrifugation is a stronger separation technique and causes a dense pellet of nanoparticles to form, whereas magnetic separation results in a less dense collection of nanoparticles in the sample tubes.

Overall, the solutions with the magnetically separated nanoparticles resulted in higher viscosity values that those with centrifuged nanoparticles. This result may be due to a larger amount of residual water molecules that remain adsorbed to the nanoparticle surfaces in the magnetically separated samples versus the centrifuged samples. In addition, the magnetically separated nanoparticles may be more easily redispersed in DMAC once the synthesis solution is removed, resulting in less particle agglomeration. Both explanations would result in an increase in solution viscosity. In the first case, water molecules act similarly to ethanol as a solution additive that would increase solution viscosity. In the second case, better nanoparticle dispersion would cause the polymer solution to be exposed to more of the nanoparticles, and the well-dispersed nanoparticles will have a greater effect on viscosity than in samples where some of the particles are still agglomerated. Similar to the results shown in Fig. 3, ATMP-stabilized nanoparticles generally resulted in higher viscosities than CMC-stabilized nanoparticles, with several exceptions.

Resulting membrane thickness is shown in Fig. 7 for both stabilizer types and the two separation techniques. Generally, membranes separated by centrifugation resulted in slightly higher membrane thickness, compared to the membranes containing magnetically separated nanoparticles. A summary of FESEM images for the cast membranes reported in Fig. 7 can be found in Supplemental Material.

Pure water flux was evaluated for the two different separation techniques, and results are shown in Fig. 8. Except for a few cases, the membranes containing nanoparticles separated by centrifugation resulted in higher pure water flux measurements. The type of stabilizer appears to affect the flux results as well, but there is no clear trend in terms of casting solution composition and nanoparticle separation method. Further delineation of these different parameters would require a larger sample set with additional compositions, as well as a comparison to other stabilizers that have specific differences in molecular structure or functional groups (e.g., different CMC polymer molecular weights or degrees of substitution of carboxymethyl groups, or other phosphonate chelators with different numbers of phosphate groups).

4. Conclusions

In this study, the roles of nanoparticle stabilizer type, casting solution additives ethanol and PVP, and post-synthesis nanoparticle processing in PES membrane properties were evaluated. Iron nanoparticles were synthesized with either ATMP or CMC as the stabilizer, and nanoparticle morphology and size were similar. Membrane casting solutions were characterized using viscosity measurements, and cast membranes were evaluated for thickness and pure water flux. The addition of ethanol and PVP as casting solution additives caused expected increases in casting solution viscosity, which can be explained by the decrease in solvent volume available to dissolve PES with the addition of the additives. However, the addition of stabilized iron nanoparticles caused either an increase or decrease in casting solution viscosity, depending on the composition of the casting solution and the type of stabilizer used. In the presence of the additive ethanol at concentrations of 1 wt % to 15 wt %, ATMP-stabilized iron nanoparticles caused the viscosity to increase, compared to the nanoparticle-free casting solution, while the addition of CMC-stabilized iron nanoparticles caused the viscosity to decrease. At 25 wt % ethanol, the effect of the stabilizer type switches, and CMC causes an increase in viscosity. When 2 wt % PVP is added, nanoparticle addition causes the viscosity to decrease for all ethanol concentrations tested. Viscosity changes as
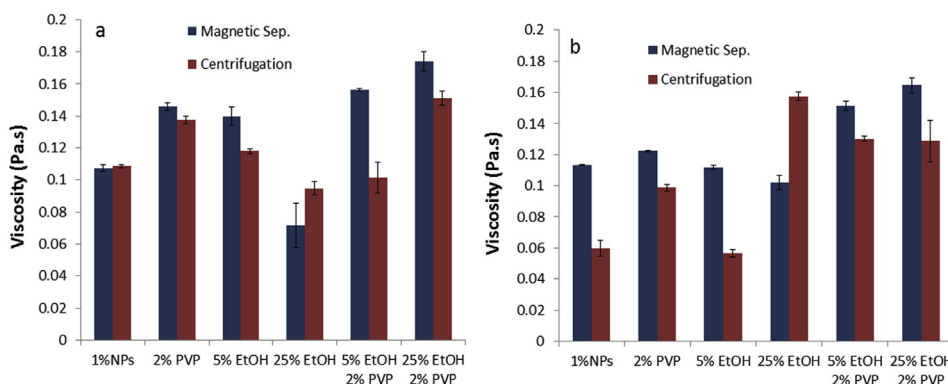

Fig. 6. Effect of nanoparticle separation technique on casting solution viscosity. Nanoparticles stabilized by (a) ATMP or (b) CMC were separated from the synthesis solution by either magnetic separation or centrifugation and then resuspended in DMAC and 15% PES. Several solutions contained PVP and/or ethanol as additives. All experiments were run at 20 °C.
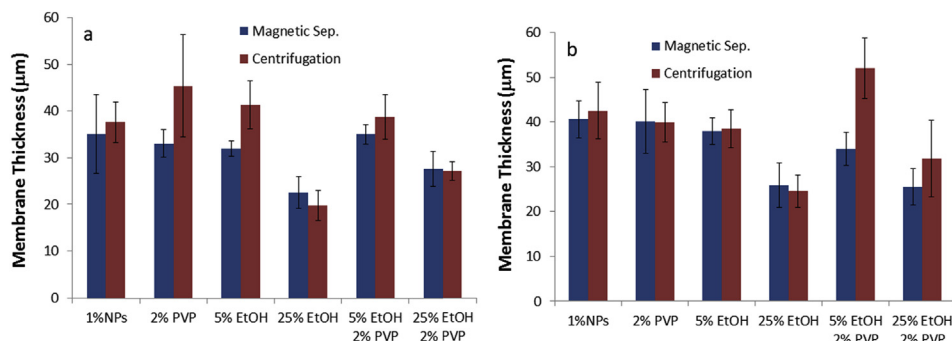
Fig. 7. Effect of nanoparticle separation technique on cast membrane thickness. Nanoparticles stabilized by (a) ATMP or (b) CMC were separated from the synthesis solution by either magnetic separation or centrifugation and then resuspended in DMAC and 15% PES.
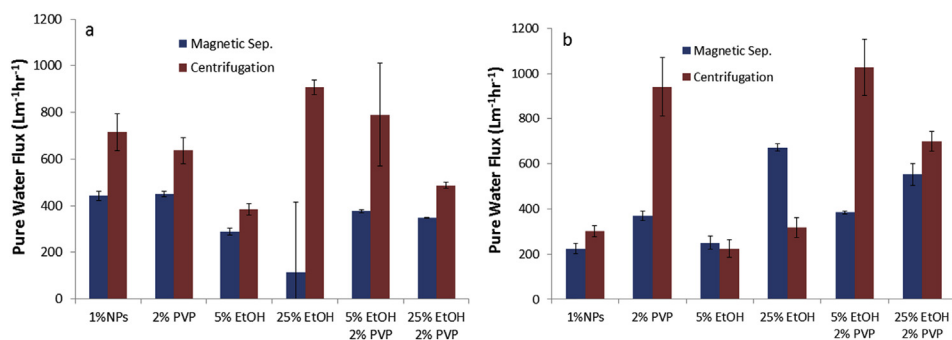

Fig. 8. Effect of nanoparticle separation technique on membrane pure water flux. Nanoparticles are stabilized by (a) ATMP or (b) CMC.

a function of ethanol concentration resulted in different trends depending on the stabilizer type and the presence or absence of PVP. Membrane thickness changes are likely related to changes in the viscosity, and the resulting changes in the thermodynamic stability and kinetics of phase inversion. Pure water flux decreases for all nanoparticle-embedded membranes, but the difference between the flux of nanoparticle-free and nanoparticle-embedded membranes varies significantly depending on casting solution composition and stabilizer type.

When nanoparticles are separated by centrifugation versus magnetic separation post-synthesis, the resulting casting solution viscosity, membrane thickness and pure water flux are affected. Magnetic separation largely results in higher viscosity measurements and slightly lower membrane thickness values. Pure water flux measurements suggest centrifugal separation of the nanoparticles from the synthesis solution allows higher water flux than magnetic separation. FESEM images of membranes (Supplemental Material) illustrate differences in the thickness of the dense polymer layer at the top surface of the membrane as well as differences in the internal macrovoid structure.

Appendix A. Supplementary data

Supplementary data related to this article can be found at http://dx.doi.org/10.1016/j.polymer.2016.04.021.

References

[1] A. Gholami, A.R. Moghadassi, S.M. Hosseini, S. Shabani, F. Gholami, Preparation and characterization of polyvinyl chloride based nanocomposite nanofiltration-membrane modified by iron oxide nanoparticles for lead removal from water, J. Ind. Eng. Chem. 20 (2014) 1517–1522.
[2] M. Tong, S. Yuan, H. Long, M. Zheng, L. Wang, J. Chen, Reduction of nitrobenzene in groundwater by iron nanoparticles immobilized in PEG/nylon membrane, J. Contam. Hydrol. 122 (2011) 16–25.
[4] P. Daraei, S.S. Madaeni, N. Ghaemi, E. Salehi, M.A. Khadivi, R. Moradian, B. Astinchap, Novel polyethersulfone nanocomposite membrane prepared by PANI/Fe$_3$O$_4$ nanoparticles with enhanced performance for Cu(II) removal from water, J. Membr. Sci. 415–416 (2012) 250–259.
[5] Y. Georgiou, K. Dimos, K. Beltsios, M.A. Karakassides, Y. Deligiannakis, Hybrid [polysulfone–Zero Valent Iron] membranes: Synthesis, characterization and application for As^{III} remediation, Chem. Eng. J. 281 (2015) 651–660.
[6] G.K. Parshetti, R.-a. Doong, Dechlorination of chlorinated hydrocarbons by bimetallic Ni/Fe immobilized on polyethylene glycol-grafted microfiltration membranes under anoxic conditions, Chemosphere 86 (2012) 392–399.
[7] P. Daraei, S.S. Madaeni, N. Ghaemi, M.A. Khadivi, B. Astinchap, R. Moradian, Fouling resistant mixed matrix polyethersulfone membranes blended with magnetic nanoparticles: Study of magnetic field induced casting, Sep. Purif. Technol. 109 (2013) 111–121.
[8] S. Balta, A. Sotto, P. Luis, L. Benea, B. Van der Bruggen, J. Kim, A new outlook on membrane enhancement with nanoparticles: The alternative of ZnO, J. Membr. Sci. 389 (2012) 155–161.
[9] N. Ghaemi, S.S. Madaeni, P. Daraei, H. Rajabi, S. Zinadini, A. Alizadeh, R. Heydari, M. Beygzadeh, S. Ghouzivand, Polyethersulfone membrane enhanced with iron oxide nanoparticles for copper removal from water: application of new functionalized Fe$_3$O$_4$ nanoparticles, Chem. Eng. J. 263 (2015) 101–112.
[10] M. Mukherjee, S. De, Reduction of microbial contamination from drinking water using an iron oxide nanoparticle-impregnated ultrafiltration mixed matrix membrane: preparation, characterization and antimicrobial properties, Environ. Sci. Water Res. 1 (2015) 204–217.
[11] N.G. Moustakas, F.K. Katsaros, A.G. Kontos, G.E. Romanos, D.D. Dionysiou, P. Falaras, Visible light active TiO$_2$ photocatalytic filtration membranes with improved permeability and low energy consumption, Catal. Today 224 (2014) 56–69.
[12] V.S. Coker, A. Garrity, W.B. Wennekes, H.D.W. Roesink, R.S. Cutting, J.R. Lloyd, Cr(VI) and azo dye removal using a hollow-fibre membrane system functionalized with a biogenic Pd-magnetite catalyst, Environ. Technol. 35 (2014) 1046–1054.
[13] C. Liu, X. Li, B. Ma, A. Qin, C. He, Removal of water contaminants by nanoscale zero-valent iron immobilized in PAN-based oxidized membrane, Appl. Surf. Sci. 321 (2014) 158–165.
[14] S. Zinadini, A.A. Zinatizadeh, M. Rahimi, V. Vatanpour, H. Zangeneh, M. Beygzadeh, Novel high flux antifouling nanofiltration membranes for dye removal containing carboxymethyl chitosan coated Fe3O4 nanoparticles, Desalination 349 (2014) 145–154.
[15] Y. Xie, R. Sougrat, S.P. Nunes, Synthesis and characterization of polystyrene

coated iron oxide nanoparticles and asymmetric assemblies by phase inversion, J. Appl. Polym. Sci. 132 (2015) 41368.

[16] R. Saranya, G. Arthanareeswaran, A.F. Ismail, D.D. Dionysiou, D. Paul, Zero-valent iron impregnated cellulose acetate mixed matrix membranes for the treatment of textile industry effluent, RSC Adv. 5 (2015) 62486–62497.

[17] J. Yang, X. Wang, M. Zhu, H. Liu, J. Ma, Investigation of PAA/PVDF–NZVI hybrids for metronidazole removal: Synthesis, characterization, and reactivity characteristics, J. Hazard. Mater. 264 (2014) 269–277.

[18] J. Fan, Y. Guo, J. Wang, M. Fan, Rapid decolorization of azo dye methyl orange in aqueous solution by nanoscale zerovalent iron particles, J. Hazard. Mater. 166 (2009) 904–910.

[19] Z. Fang, X. Qiu, J. Chen, X. Qiu, Debromination of polybrominated diphenyl ethers by Ni/Fe bimetallic nanoparticles: Influencing factors, kinetics, and mechanism, J. Hazard. Mater. 185 (2011) 958–969.

[20] A. Ryu, S.-W. Jeong, A. Jang, H. Choi, Reduction of highly concentrated nitrate using nanoscale zero-valent iron: Effects of aggregation and catalyst on reactivity, Appl. Catal. B 105 (2011) 128–135.

[21] D.R. Petkar, B.S. Kadu, R.C. Chikate, Highly efficient and chemoselective transfer hydrogenation of nitroarenes at room temperature over magnetically separable Fe-Ni bimetallic nanoparticles, RSC Adv. 4 (2014) 8004.

[22] D. Nandi, K. Gupta, A.K. Ghosh, A. De, S. Banerjee, U.C. Ghosh, Manganese-incorporated iron(III) oxide-graphene magnetic nanocomposite: synthesis, characterization, and application for the arsenic(III)-sorption from aqueous solution, J. Nanopart. Res. 14 (2012) 149–162.

[23] C.-C. Huang, H.-L. Lien, Trimetallic Pd/Fe/Al particles for catalytic dechlorination of chlorinated organic contaminants, Water Sci. Technol. 62 (2010) 202–208.

[24] J. Cao, R. Xu, H. Tang, S. Tang, M. Cao, Synthesis of monodispersed CMC-stabilized Fe-Cu bimetal nanoparticles for in situ reductive dechlorination of 1, 2, 4-trichlorobenzene, Sci. Total Environ. 409 (2011) 2336–2341.

[25] J. Wang, C. Liu, L. Tong, J. Li, R. Luo, J. Qi, Y. Li, L. Wang, Iron-copper bimetallic nanoparticles supported on hollow mesoporous silica spheres: an effective heterogeneous Fenton catalyst for orange II degradation, RSC Adv. 5 (2015) 69593–69605.

[26] X. Wang, L. Le, P.J.J. Alvarez, F. Li, K. Liu, Synthesis and characterization of green agents coated Pd/Fe bimetallic nanoparticles, J. Taiwan Inst. Chem. Eng. 50 (2015) 297–305.

[27] F. Luo, D. Yang, Z. Chen, M. Megharaj, R. Naidu, The mechanism for degrading Orange II based on adsorption and reduction by iron-based nanoparticles synthesized by grape leaf extract,, J. Hazard. Mater. 296 (2015) 37–45.

[28] T. Wang, X. Jin, Z. Chen, M. Megharaj, R. Naidu, Green synthesis of Fe nanoparticles using eucalyptus leaf extracts for treatment of eutrophic wastewater, Sci. Total Environ. 466–467 (2014) 210–213.

[29] Y. Xie, Z. Fang, W. Cheng, P.E. Tsang, D. Zhao, Remediation of polybrominated diphenyl ethers in soil using Ni/Fe bimetallic nanoparticles: Influencing factors, kinetics and mechanism, Sci. Total Environ. 485–486 (2014) 363–370.

[30] Y. Han, W. Yan, Bimetallic nickel–iron nanoparticles for groundwater decontamination: Effect of groundwater constituents on surface deactivation, Water Res. 66 (2014) 149–159.

[31] J. Shi, S. Yi, H. He, C. Long, A. Li, Preparation of nanoscale zero-valent iron supported on chelating resin with nitrogen donor atoms for simultaneous reduction of Pb^{2+} and NO_3^-, Chem. Eng. J. 230 (2013) 166–171.

[32] B. Kakavandi, R.R. Kalantary, M. Farzadkia, A.H. Mahvi, A. Esrafili, A. Azari, A.R. Yari, A.B. Javid, Enhanced chromium (VI) removal using activated carbon modified by zero valent iron and silver bimetallic nanoparticles, J. Environ. Health Sci. Eng. 12 (2014) 115.

[33] F. Fu, Z. Cheng, D.D. Dionysiou, B. Tang, Fe/Al bimetallic particles for the fast and highly efficient removal of Cr(VI) over a wide pH range: Performance and mechanism, J. Hazard. Mater. 298 (2015) 261–269.

[34] G. Asgarai, B. Ramavandi, S. Farjadfard, Abatement of azo dye from wastewater using bimetal-chitosan, Sci. World J. 2013 (2013) 476271.

[35] V.K. Gupta, N. Atar, M.L. Yola, Z. Üstündağ, L. Uzun, A novel magnetic Fe@Au core–shell nanoparticles anchored graphene oxide recyclable nanocatalyst for the reduction of nitrophenol compounds, Water Res. 48 (2014) 210–217.

[36] W.-J. Liu, T.-T. Qian, H. Jiang, Bimetallic Fe nanoparticles: Recent advances in synthesis and application in catalytic elimination of environmental pollutants, Chem. Eng. J. 236 (2014) 448–463.

[37] D. O'Carroll, B. Sleep, M. Krol, H. Boparai, C. Kocur, Nanoscale zero valent iron and bimetallic particles for contaminated site remediation, Adv. Water Res. 51 (2013) 104–122.

[38] N. Maximous, G. Nakhla, W. Wan, K. Wong, Performance of a novel ZrO2/PES membrane for wastewater filtration, J. Membr. Sci. 352 (2010) 222–230.

[39] P.S. Goh, B.C. Ng, W.J. Lau, A.F. Ismail, Inorganic nanomaterials in polymeric ultrafiltration membranes for water treatment, Sep. Purif. Rev. 44 (2015) 216–249.

[40] S. Rajesh, S. Senthilkumar, A. Jayalakshmi, M.T. Nirmala, A.F. Ismail, D. Mohan, Preparation and performance evaluation of poly (amide-imide) and TiO2 nanoparticles impregnated polysulfone nanofiltration membranes in the removal of humic substances, Colloids Surf. A Physicochem. Eng. Asp. 418 (2013) 92–104.

[41] H.R. Pant, H.J. Kim, M.K. Joshi, B. Pant, C.H. Park, J.I. Kim, K.S. Hui, C.S. Kim, One-step fabrication of multifunctional composite polyurethane spider-web-like nanofibrous membrane for water purification, J. Hazard. Mater. 264 (2014) 25–33.

[42] C.P. Leo, W.P. Cathie Lee, A.L. Ahmad, A.W. Mohammad, Polysulfone

[43] N. Akar, B. Asar, N. Dizge, I. Koyuncu, Investigation of characterization of biofouling properties of PES membrane containing selenium and copper nanoparticles, J. Membr. Sci. 437 (2013) 216–226.

[44] B. Baruwati, R.S. Varma, High value products from waste: Grape pomace extract-A three-in-one package for the synthesis of metal nanoparticles, ChemSusChem 2 (2009) 1041–1044.

[45] F. He, D. Zhao, Preparation and characterization of a new class of starch-stabilized bimetallic nanoparticles for degradation of chlorinated hydrocarbons in water, Environ. Sci. Technol. 39 (2005) 3314–3320.

[46] Q.G. Huang, X.Y. Shi, R.A. Pinto, E.J. Petersen, W.J. Weber, Tunable synthesis and immobilization of zero-valent iron nanoparticles for environmental applications, Environ. Sci. Technol. 42 (2008) 8884–8889.

[47] C.-h. Lin, Y.-h. Shih, J. MacFarlane, Amphiphilic compounds enhance the dechlorination of pentachlorophenol with Ni/Fe bimetallic nanoparticles, Chem. Eng. J. 262 (2015) 59–67.

[48] Y. Xie, Z. Fang, X. Qiu, E.P. Tsang, B. Liang, Comparisons of the reactivity, reusability and stability of four different zero-valent iron-based nanoparticles, Chemosphere 108 (2014) 433–436.

[49] C.-p. Tso, Y.-h. Shih, The reactivity of well-dispersed zerovalent iron nanoparticles toward pentachlorophenol in water,, Water Res. 72 (2015) 372–380.

[50] C.-C. Huang, S.-L. Lo, H.-L. Lien, Vitamin B12-mediated hydrodechlorination of dichloromethane by bimetallic Cu/Al particles, Chem. Eng. J. 273 (2015) 413–420.

[51] M. Amirilargani, T. Mohammadi, Synthesis and characterization of asymmetric polyethersulfone membranes: effects of concentration and polarity of nonsolvent additives on morphology and performance of the membranes, Polym. Adv. Technol. 22 (2009) 962–972.

[52] R.M. Boom, I.M. Wienk, T. van den Boomgaard, C.A. Smolders, Microstructures in phase inversion membranes. Part 2. The role of a polymeric additive, J. Membr. Sci. 73 (1992) 277–292.

[53] B. Chakrabarty, A.K. Ghoshal, A.K. Purkait, Preparation, characterization and performance studies of polysulfone membranes using PVP as an additive, J. Membr. Sci. 315 (2008) 36–47.

[54] M.-J. Han, S.-T. Nam, Thermodynamic and rheological variation in polysulfone solution by PVP and its effect in the preparation of phase inversion membrane, J. Membr. Sci. 202 (2002) 55–61.

[55] B. Jung, J.K. Yoon, B. Kim, H.-W. Rhee, Effect of molecular weight of polymeric additives on formation, permeation properties, and hypochlorite treatment of asymmetric polyacrylonitrile membranes, J. Membr. Sci. 243 (2004) 45–47.

[56] L.Y. Lafrenière, F.D.F. Talbot, T. Matsuura, S. Sourirajan, Effect of polyvinylpyrrolidone additive on the performance of polyethersulfone ultrafiltration membranes, Ind. Eng. Chem. Res. 26 (1987) 2385–2389.

[57] N. Goldstein, L.F. Greenlee, Influence of synthesis parameters on iron nanoparticle size and zeta potential, J. Nanopart. Res. 14 (2012) 760.

[58] L.F. Greenlee, N.S. Rentz, ATMP-stabilized iron nanoparticles: chelator-controlled nanoparticle synthesis, J. Nanopart. Res. 16 (2014) 2712.

[59] K. Sawada, W.B. Duan, M. Ono, K. Satoh, Stability and structure of nitrilo(acetate-methylphosphonate) complexes of the alkaline-earth and divalent transition metal ions in aqueous solution, J. Chem. Dalt. Trans. (2000) 919–924.

[60] L.F. Greenlee, J.D. Torrey, R.L. Amaro, J.M. Shaw, Kinetics of zero valent iron nanoparticle oxidation in oxygenated water, Environ. Sci. Technol. 46 (2012) 12913–12920.

[61] C.-t.F. Lo, K. Karan, B.R. Davis, Kinetic studies of reaction between sodium borohydride and methanol, water, and their mixtures, Ind. Eng. Chem. Res. 46 (2007) 5478–5484.

[62] B. An, D. Zhao, Immobilization of As(III) in soil and groundwater using a new class of polysaccharide stabilized Fe-Mn oxide nanoparticles, J. Hazard. Mater. 211–212 (2012) 332–341.

[63] H. Dong, Y. Xie, G. Zeng, L. Tang, J. Liang, Q. He, F. Zhao, Y. Zeng, Y. Wu, The dual effects of carboxymethyl cellulose on the colloidal stability and toxicity of nanoscale zero-valent iron,, Chemosphere 144 (2016) 1682–1689.

[64] F. He, D. Zhao, C. Paul, Field assessment of carboxymethyl cellulose stabilized iron nanoparticles for in situ destruction of chlorinated solvents in source zones, Water Res. 44 (2010) 2360–2370.

[65] F. He, D.Y. Zhao, Manipulating the size and dispersibility of zerovalent iron nanoparticles by use of carboxymethyl cellulose stabilizers, Environ. Sci. Technol. 41 (2007) 6216–6221.

[66] C. Chen, P. Gunawan, R. Xu, Self-assembled Fe3O4-layered double hydroxide colloidal nanohybrids with excellent performance for treatment of organic dyes in water, J. Mater. Chem. 21 (2010) 1218–1225.

[67] K.O. Abdulwahab, M.A. Malik, P. O'Brien, G.A. Timco, A direct synthesis of water soluble monodisperse cobalt and manganese ferrite nanoparticles from iron based pivalate clusters by the hot injection thermolysis method,, Mater. Sci. Semicond. Process. 27 (2014) 303–308.

[68] K.J. Carroll, D.M. Hudgins, L.W. Brown, S.D. Yoon, D. Heiman, V.G. Harris, E.E. Carpenter, Annealing of amorphous FexCo100-x nanoparticles synthesized by a modified aqueous reduction using NaBH4, J. Appl. Phys. 107 (2010) 3.

[69] L.F. Greenlee, S. Hooker, Characterization of stabilized zero valent iron nanoparticles, in: T. Boellinghaus, J. Lexow, T. Kishi, M. Kitagawa (Eds.), Materials Challenges and Testing for Supply of Energy and Resources, Springer Verlag, Berlin, Germany, 2012, pp. 173–188.

[70] L.F. Greenlee, S.A. Hooker, Development of stabilized zero valent iron

nanoparticles, Desalin. Water Treat. 37 (2012) 114–121.

[71] P.A. Chernavskii, N.V. Peskov, A.V. Mugtasimov, V.V. Lunin, Oxidation of metal nanoparticles: Experiment and model, Russ. J. Phys. Chem. B 1 (2007) 394–411.

[72] B.T. Swinyard, J.A. Barrie, Phase separation in non-solvent/dimethylformamide/polyethersulphone and non-solven/dimethylformamide/polysulphone systems, Brit. Polym. J. 20 (1988) 317–321.

[73] M. Doi, S.F. Edwards, Dynamics of concentrated polymer systems. Part 1.- Brownian motion in the equilibrium state, J. Chem. Soc. Faraday Trans. 2 Molec. Chem. Phys. 74 (1978) 1789–1801.

[74] W.-F. Su, Polymer size and polymer solutions, in: Principles of Polymer Design and Synthesis, Springer, Berlin Heidelberg, 2013, pp. 9–26. Berlin, Heidelberg.

[75] N.B. Wyatt, M.W. Liberatore, Rheology and viscosity scaling of the polyelectrolyte xanthan gum, J. Appl. Polym. Sci. 114 (2009) 4076–4084.

[76] M.W. Donnelly, M. Hailemichael, M.W. Liberatore, Altering the viscosity of cationically modified cellulose polymers by the addition of salt, J. Appl. Polym. Sci. (2014) 41616.

[77] P. Aerts, E. Van Hoof, R. Leysen, I.F.J. Vankelecom, P.A. Jacobs, Polysulfone-Aerosil composite membranes – part 1. The influence of the addition of Aerosil on the formation process and membrane morphology, J. Membr. Sci. 176 (2000) 63–73.

[78] B. Torrestiana-Sanchez, R.I. Ortiz-Basurto, E. Brito-De La Fuente, Effect of nonsolvents on properties of spinning solutions and polyethersulfone hollow fiber ultrafiltration membranes, J. Membr. Sci. 152 (1999) 19–28.

[79] S.K. Zaidi, A. Kumar, Effects of ethanol concentration on flux and gel formation in dead end ultrafiltration of PEG and dextran, J. Membr. Sci. 237 (2004) 189–197.

[80] K. Wang, Description of extrudate swell for polymer nanocomposites, Materials 3 (2010) 386–400.

[81] K. Wang, Die swell of complex polymeric systems, in: J. De Vicente (Ed.), Viscoelasticity – From Theory to Biological Applications, InTech, 2012. http://dx.doi.org/10.5772/50137.

[82] C. Barth, M.C. Goncalves, A.T.N. Pires, J. Roeder, B.A. Wolf, Asymmetric polysulfone and polyethersulfone membranes: effects of thermodynamic conditions during formation on their performance, J. Membr. Sci. 169 (2000) 287–299.

[83] K. Kimmerle, H. Strathmann, Analysis of the structure-determining process of phase inversion membranes, Desalination 79 (1990) 283–302.

[84] A. Rahimpour, S.S. Madaeni, A.H. Taheri, Y. Mansourpanah, Coupling TiO₂ nanoparticles with UV irradiation for modification of polyethersulfone ultrafiltration membranes, J. Membr. Sci. 313 (2008) 158–169.

[85] X. Bai, Y. Zhang, H. Wang, H. Zhang, J. Liu, Study on the modification of positively charged composite nanofiltration membrane by TiO₂ nanoparticles, Desalination 313 (2013) 57–65.

[86] H. Strathmann, K. Kock, The formation mechanism of phase inversion membranes, Desalination 21 (1977) 241–255.

[87] V.C. Souza, M.G.N. Quadri, Organic-inorganic hybrid membranes in separation processes: A 10-year review, Braz. J. Chem. Eng. 30 (2013) 683–700.

[88] O. Bakhtiari, N. Sadeghi, Mixed matrix membranes' gas separation performance prediction using an analytical model, Chem. Eng. Res. Des. 93 (2015) 710–719.

[89] A. Shariati, M. Omidkhah, M.Z. Pedram, New permeation models for nano-composite polymeric membranes filled with nonporous particles, Chem. Eng. Res. Des. 90 (2012) 563–575.